



EXPERIMENTAL STUDIES ON FULL-SCALE POST-TENSIONED STEEL MOMENT CONNECTIONS

Maria GARLOCK¹, James M. RICLES², Richard SAUSE³

SUMMARY

Six full-scale interior connection subassemblies of post-tensioned wide flange beam-to-column moment connections were tested. Each was subjected to inelastic cyclic loading up to 4% story drift to simulate earthquake loading effects. Bolted top and seat angles are used in the connection, along with post-tensioned high strength strands that run parallel to the beam. These strands compress the beam flanges against the column flange to develop the resisting moment to service loading and to provide a restoring force that returns the structure to its pre-earthquake position. The parameters studied in these experiments were the initial post-tensioning force, the number of post-tensioning strands, and the length of the reinforcing plates. The experimental results demonstrate that the post-tensioned connection possesses good energy dissipation and ductility. Under drift levels of 4%, the beams and columns remain elastic, while only the top and seat angles are damaged and dissipate energy. The lack of damage to the beams, columns, and the post-tensioning enable the system to return to its plumb position (i.e., it self centers). Closed-form expressions are presented to predict the connection response and the results from these expressions compare well with the experimental results.

INTRODUCTION

Structural steel has been widely used in moment resisting frame (MRF) systems for buildings. The connections in steel MRFs are either welded or bolted, with welding becoming common during recent decades. A typical welded moment connection detail consists of a bolted shear tab with full penetration beam flange welds. During the 1994 Northridge earthquake, many steel MRFs suffered unexpected premature connection fractures. Several alternative moment connection details have been proposed since the Northridge earthquake [1] in an attempt to develop ductile response under earthquake loading. These details are intended to avoid weld failure and force inelastic deformation to develop in the beams away from the welds. Consequently, after a design-level earthquake, the beams with these connections will have permanent damage caused by yielding and local buckling. This damage can result in a significant residual drift of the MRF.

¹ Assistant Professor, Dept. of Civil and Environmental Engineering, Princeton University

² Bruce G. Johnson Professor of Structural Engineering, Dept. of Civil and Environmental Eng., Lehigh University

³ Joseph T. Stuart Professor of Engineering, Dept. of Civil and Environmental Eng., Lehigh University

As an alternative to welded construction the authors developed a post-tensioned (PT) moment connection for use in seismic resistant steel MRFs. The connection utilizes high strength steel strands that are post-tensioned after bolted top-and-seat angles are installed (Figure 1(a)). The post-tensioning strands run through the columns, and are anchored against the column flange (Figure 1(b)). A properly designed PT connection has several advantages: (1) field welding is not required; (2) the connection is made with conventional materials and skills; (3) the connection has an initial stiffness similar to that of a typical welded connection; (4) the connection is self-centering without residual deformation, thus the MRF will not have residual drift after an earthquake if significant residual deformation does not occur at the base of the columns; (5) the beams and columns remain essentially elastic while inelastic deformation of the top-and-seat angles provides energy dissipation; (6) the angles are easily replaced, and (7) the system is redundant, for the vertical shear is supported by both the angles and the friction between the beam and the column, and since the system uses several PT strands the system continues to function even if failure of one or more strands occurs.

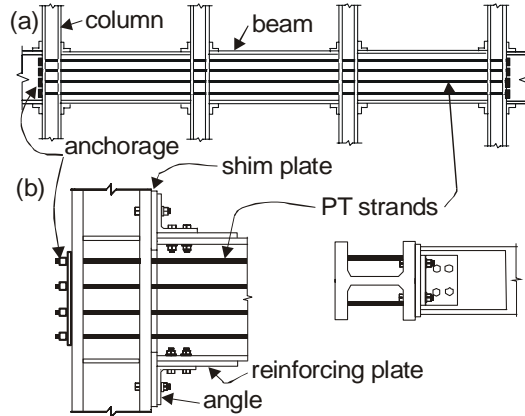


Figure 1. (a) Schematic elevation of one floor of a PT frame and (b) connection details.

This paper presents experimental studies of six full-scale PT connection subassemblies subjected to cyclic inelastic loading. Each specimen represents an interior connection and consists of W36x150 beams attached to a W14x398 column. The parameters investigated in the study include the number of PT strands and the initial post-tensioning force. These parameters are chosen so that different limit states would occur including angle fracture, strand yielding, and beam local buckling. This paper is a summary of Garlock et al. [2]. Garlock et al. [3] describes the design and seismic behavior of steel frames with PT connections.

BACKGROUND

Post-tensioned Connection Description

The PT steel MRF connection studied includes bolted top-and-seat angles, attached to the beam and column flanges, and seven-wire ASTM A-416 high strength stress relieved strands running parallel to the beam and anchored outside the connection (see Figure 1(a)). The strands compress the beam flanges against the column flanges to resist moment, while the two angles and the friction at the beam and column interface resist transverse shear force. The proposed details are shown in Figure 1(b) for a connection to an exterior column. The angles' primary purpose is to dissipate energy. However, they also provide redundancy to the force transfer mechanisms for transverse beam shear and beam end moment. Reinforcing plates are welded to the beam flanges to control beam yielding. Also, shim plates are placed between the column flange and the beam flanges so that only the beam flanges and reinforcing plates are in contact with the column.

The idealized moment-rotation ($M-\theta_r$) behavior of a PT steel connection is shown in Figure 2(a), where θ_r is the relative rotation between the beam and column (as shown in Figure 2(b)). The $M-\theta_r$ behavior of a PT connection is characterized by gap opening, Δ_{gap} , and closing at the beam-column interface under cyclic loading (Figure 2(b)). The moment to initiate this separation is called the decompression moment. The connection behavior is initially similar to a welded moment connection, but following decompression

the behavior is similar to a partially restrained connection. The initial stiffness of the connection is the same as that of a welded moment connection before the gap opens at decompression (while θ_r equals zero before event 1 in Figure 2(a)). The stiffness of the connection after decompression is associated with the stiffness of the angles and the elastic axial stiffness of the post-tensioned strands. With continued loading, the tension angle of the connection yields (event 2), with full plastic yielding of the tension angle at event 3. With continued loading, the strands will yield eventually at event 5. The M - θ_r relationship has a nearly linear response between events 3 and 5 where the connection stiffness is primarily due to the axial stiffness of the PT strands. Upon unloading (event 4), the angles will dissipate energy (between events 4 and 8) until the gap between the beam flange and the column face is closed at event 8 (i.e., when θ_r is equal to zero). A complete reversal in applied moment will result in similar connection behavior occurring in the opposite direction of loading, as shown in Figure 2(a).

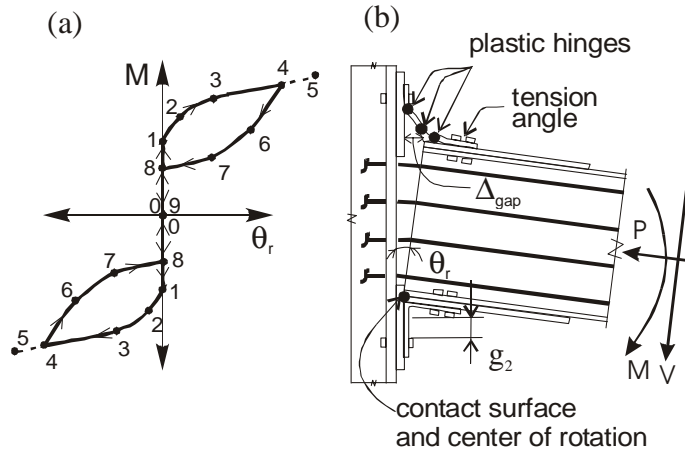


Figure 2. (a) Moment-rotation behavior, and (b) deformation of a decompressed PT connection.

The flexural strength of a PT connection depends on the total strand force, the strength of the angles, and the elastic stiffness and strength of the post-tensioning strands. As long as the strands remain elastic and there is no significant beam yielding, the post-tensioning force is preserved and the connection will self-center upon unloading (i.e., θ_r returns to zero upon removal of the connection moment and the MRF returns to its pre-earthquake position). The energy dissipation capacity of the connection is related to the flexural strength of the angles. Garlock et al. [4] shows that the tension angle develops a mechanism by the formation of three plastic hinges (see Figure 2(b)): one plastic hinge forms on the fillet of each angle leg, and another near the bolts connecting the angle to the column (column bolts).

Prior Research

Cheok and Lew [5] and Cheok and Stone [6] experimentally studied beam-column joint subassemblies with PT connections for precast concrete frame structures. They found that the PT concrete connection performs well and that the performance was enhanced when mild (non prestressed) steel reinforcement was provided for energy dissipation. El-Sheikh et al. [7] conducted an analytical study of the seismic behavior of unbonded PT precast concrete frames. Although the system studied by El-Sheikh et al. did not include a component specifically intended for energy dissipation (such as mild steel), they found that the system performs reasonably well, even while dissipating little energy.

Rojas et al. [8, 9] studied a PT connection for steel MRFs with connection details similar to those described in this paper, except that their connection uses friction devices to dissipate energy (in lieu of top-and-seat angles). The research by Rojas et al. included several nonlinear time-history analyses of steel frames with PT connections as well as steel frames with welded connections. Results show good energy dissipation, strength and ductility in the PT frame, and the response of the PT frame can exceed that of a frame with rigid connections. Christopoulos et al. [10, 11, 12] performed analytical and experimental studies on a PT steel connection with details that differ from those described in this paper. The PT connection studied by Christopoulos et al. incorporates high strength steel PT bars and confined energy dissipating bars designed to yield in tension and compression. Results showed that, following large story

drifts, the system returns to its initial position without damage to the beams and columns. Christopoulos et al. [13] analytically compared the seismic response of SDOF systems incorporating flag-shaped hysteretic behavior with self-centering capability (representing PT connections) to SDOF systems with bilinear elastoplastic hysteretic behavior (representing welded connections). An ensemble of 20 earthquake records was used and it was found that the response of a flag-shaped hysteretic SDOF system matches or exceeds the response of an elastoplastic hysteretic SDOF system.

Ricles et al. [14] experimentally investigated nine steel beam-column joint subassemblies with PT connections similar to those described in this paper. The main parameter considered in this study was the angle geometry. Ricles et al. also conducted nonlinear time-history analyses of a steel frame with PT connections. The results indicate that the PT steel connection is a viable alternative to a welded connection.

The research presented in the present paper expands the work done by Ricles et al. [14]. The scope of previous research by Ricles et al. [14, 15] was limited by the connection parameters studied. The experimental investigations [14] made clear the need for reinforcing plates and shim plates in the connection, therefore these plates are included in the connections investigated in the present paper. Furthermore, the previous experiments used W24 beams, while the experiments described in this paper use much larger W36 beams. It was found that this increase in beam size changes the connection design considerably. For example, where a connection for a W24 beam requires 8 strands, a similar connection for a W36 beam requires 36 strands to reach the same connection moment relative to the plastic moment capacity of the beam.

SIMPLIFIED ANALYSIS OF PT CONNECTION BEHAVIOR

A simplified analysis of the behavior of a PT connection can be made using the free-body diagram shown in Figure 3. To make the free body, a cut is made through the fillet of the tension angle (where a plastic hinge forms), the fillet of the other angle, and at the contact surface of the beam compression flange. It is seen that the primary forces contributing to the moment developed in a PT connection are the tension angle shear force (V_a), the moments in the tension angle and compression angle (M_a^C and M_a^T , respectively) at the plastic hinge locations, and the contact force (C). The forces V_a and C are in horizontal equilibrium with the beam axial force (P). P is comprised of the sum of the strand forces (T) plus an additional axial force in the beams produced by the interaction of the PT frame with the floor diaphragm (F_{fd}). F_{fd} is explained in further detail by Garlock [16]. The strands are assumed to be horizontally oriented with the centroid of the strands located at the centroid of the beam. V_a is assumed to act at the location of the plastic hinge on the column leg fillet of the tension angle and at a distance of d_1 from the center of rotation. C is assumed to act at the center of rotation, at the compression flange and equals the axial force in the beam, P , plus V_a .

By summing moments about the beam centroid, the moment developed in a PT steel connection is given by the following equation:

$$M = (d_1 - d_2)V_a + Cd_2 + M_a^T + M_a^C \quad (1)$$

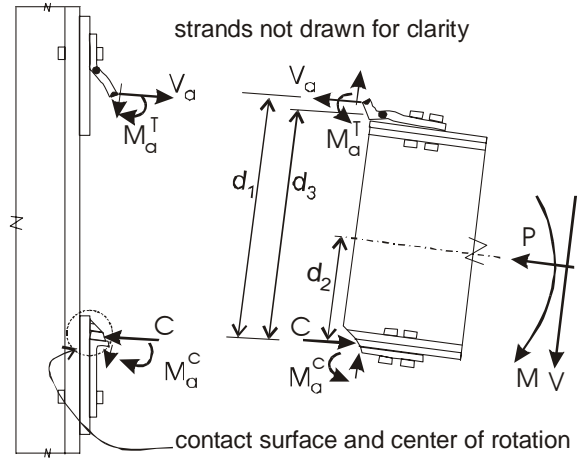


Figure 3. Free-body diagram of PT connection.

By substituting $C = T + F_{fd} + V_a$ into the above equation,

$$M = d_1 V_a + (T + F_{fd}) d_2 + M_a^T + M_a^C \quad (2)$$

Decompression of the connection occurs when the contact force resultant in the beam tension flange is zero. The theoretical decompression moment is obtained from Equation 2. Assuming F_{fd} equals zero, T equals the initial strand force sum (T_o), and V_a , M_a^T , and M_a^C are zero because θ_r is zero, the theoretical decompression moment is

$$M_{d.th} = d_c \frac{T_o}{2} \quad (3)$$

where d_c is equal to the distance over the depth of the beam between the centroids of the contact areas between the beam flanges and column (i.e., $d_c = 2d_2$). To avoid excessive drift under gravity and wind load, $M_{d.th}$ should exceed the beam end moment due to gravity and wind load.

Garlock et al. [4] performed experimental studies on sets of angles where the angle size ranged from L152x152x7.9 to L203x203x19, and the nominal yield stress ranged from 248 MPa to 345 MPa. Two angles were placed back-to-back and loaded cyclically. It was found that the angles formed a mechanism with three plastic hinges as shown in Figure 2(b). Furthermore, the angles were found to have significant strength beyond the force at which a yield mechanism occurs due to material and geometric hardening. After the mechanism forms in the angle, the following equation was found to estimate the tension angle force:

$$V_a = \underbrace{(1.13 + 0.047 \Delta_{gap})}_{\beta} \cdot \underbrace{(1.35 - 0.027t)}_{C_v} \cdot \frac{2M_{a,p}}{g_2} \quad (4)$$

where β accounts for the overstrength due to material and geometric hardening, and C_v accounts for the influence of the angle thickness, t (in units of mm) on the location of the plastic hinge near the column bolts. Δ_{gap} is the amount of gap opening (see Figure 2(b)) in units of mm. In a PT connection Δ_{gap} can be estimated as d_3 times θ_r where d_3 is the distance from the center of rotation to the tension angle leg centerline (see Figure 3). $M_{a,p}$ is the plastic moment capacity of the angle cross-section, and g_2 is the distance between the centerline of the fillet on the angle leg and the inside edge of the column bolt nut (assuming the flat edge is parallel to angle width) as shown in Figure 2(b).

Following decompression, the strands elongate producing an increase in strand force, which, in turn, causes the beam to shorten. The total PT force can be shown [16] to be equal to:

$$T_{th} = T_o + 2d_2 \left(\frac{k_s k_b}{k_b + k_s} \right) \theta_r \quad (5)$$

where k_s and k_b are the axial stiffnesses (i.e., AE/L) of the strands and beam, L equals the length of one bay. It is assumed that A , E , and L are constant for the entire length of the PT strands.

SUBASSEMBLY TESTS DESCRIPTION

Test Setup

The test setup is shown in Figure 4. The cruciform shaped subassembly with a PT moment connection simulated an interior joint of a MRF. The setup assumed that the column mid-height and beam mid-span are points of inflection in the MRF. Lateral bracing prevented out-of-plane displacement of the subassembly during testing. The specimens were braced 3048 mm and 4169 mm from each side of the column. The distance of 3048 mm complied with the bracing distance requirements in the AISC Seismic Provisions [17].

The stands were anchored at the ends of the beam against a short “anchor” column section as shown in Figure 4. These “anchor” columns are not needed in a complete MRF where the strands would be anchored at the exterior columns of the MRF, as shown in Figure 1. The strands were tensioned from the east (right hand) side where the strand anchor heads rested directly against the anchor column. On the west side, load cells bore against the anchor column. These load

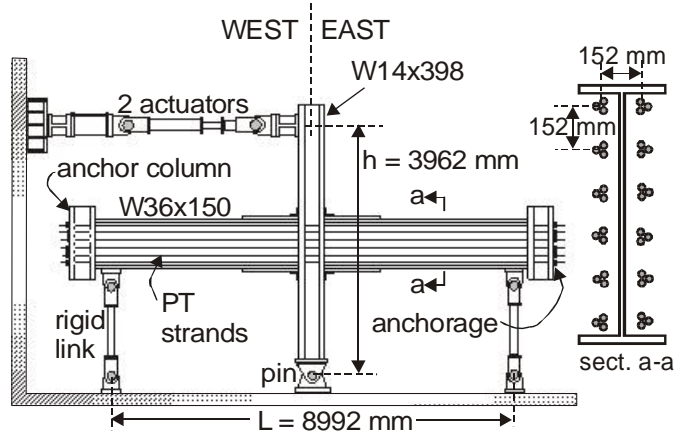


Figure 4. Test setup.

cells were placed between the strand anchor heads and the anchor column in order to measure the strand forces. For specimens with 36 strands, the strands were arranged in bundles of three, as shown in Figure 4. For specimens with fewer strands, at least one strand passed through each of the 12 holes in the column and the anchor columns. In all cases, the strands were arranged symmetrically about the beam centroid with the bundles of two or three strands nearest the centroid.

The erection of the subassembly for all specimens proceeded as follows: (1) the column was placed, (2) the beams were seated on the bottom angles that were loosely fastened to the column, (3) a good fit was ensured between the beam flanges and the shim plates at the column flange, (4) the top angles were placed and all bolts were hand tightened, (4) the strands were tensioned, and (5) the bolts in the angles were tensioned to their standard pretension force [18].

Test Specimens

Table 1 identifies the test matrix. The parameters in the test matrix included: the number of PT strands, N_s ; the total initial post-tensioning force, T_0 ; and the length of the beam flange reinforcing plates, L_{rp} . These parameters were chosen so that different limit states would occur, including angle fracture, strand yielding, and beam local buckling as shown in Table 1. In Table 1, P_y is the axial force causing yielding of the beam cross-section (i.e., nominal beam area times the nominal yield strength), and T_u is the ultimate force that the sum of the strands can carry (i.e., N_s times the ultimate force per strand). In the specimen nomenclature, the first number preceding the “s” equals N_s , and the number following the first hyphen represents the target initial force per strand (T_0/N_s) in units of kips. A “P” following a second hyphen represents the specimens with the longer reinforcing plates, and a “W” following a second hyphen represents the specimen with angles that have been welded to the beams.

Table 1 shows the sequence of the experiments. Specimen 20s-18-W was included in the test matrix after completing the test of Specimen 20s-18. Both of these specimens were expected to sustain angle fracture. Slip between the beam leg of the angle (the leg of the angle connected to the beam flange) and the beam produced impact forces in Specimen 20s-18. To evaluate if these forces caused the angles to fail prematurely, the test was repeated with Specimen 20s-18-W, which had a fillet weld between the toe of the beam leg of the angle and the beam flange.

The beam size for all the specimens was W36x150 with a 345 MPa nominal yield strength (σ_{yn}). A reinforcing plate was shop welded to the beam flanges. The first-four specimens used the same beams since no significant beam yielding occurred in the first-three tests. The fifth and sixth specimen also used the same beams. A W14x398 ($\sigma_{yn} = 345$ MPa) column was used that had shim plates shop welded to the flanges. The shim plates were 32 mm inch thick, 406 mm wide, and 292 mm long, and had a σ_{yn} of 345

MPa. All six specimens used the same column section since no significant column yielding occurred in any of the tests. The column panel zone was reinforced with 25 mm thick continuity plates and two 19 mm thick doubler plates ($\sigma_{yn} = 345$ MPa). The doubler plates were designed to keep the column panel zone elastic. The continuity plate thickness was designed to have about the same thickness as the beam flanges. The angles and bolts were replaced for each test. After some of the tests, post-tensioning strands, anchors and wedges were replaced.

Table 1. Specimen test matrix.

Specimen	N_s	T_o (kN)	L_{rp} (mm)	$\frac{T_o}{N_s}$ (kN)	$\frac{T_o}{P_y}$	$\frac{T_o}{T_u}$	Expected Limit State ^(a)
20s-18	20	1526	914	76	0.15	0.29	AF
20s-18-W	20	1312	914	66	0.13	0.25	AF
16s-45	16	3051	914	191	0.30	0.72	SY
36s-30	36	4728	914	131	0.46	0.49	BLB
36s-20-P	36	3194	1372	89	0.31	0.33	AF
36s-30-P	36	4759	1372	132	0.46	0.50	BLB

(a) AF = Angle Fracture
SY = Strand Yield
BLB = Beam Local Buckling

The reinforcing plate thickness (25 mm), width (356 mm), and steel grade ($\sigma_{yn} = 345$ MPa) remained constant in all specimens while the length, L_{rp} , varied. The reinforcing plate width and thickness were selected based on the following equation for the reinforcing plate area (A_{rp}):

$$A_{rp} \geq \frac{C - C_{f,y}}{\sigma_{rp,y}} \quad (6)$$

where C is the contact force shown in Figure 3 and described previously, $C_{f,y}$ is the beam flange yield force equal to the beam flange area times the yield stress, and $\sigma_{rp,y}$ is the reinforcing plate yield stress. Since the beams were to be reused in several specimens, and the strength of each specimen varied, a conservative value of reinforcing plate width and thickness was selected based on Equation 6.

The first four specimens had L_{rp} equal to 914 mm, while the remaining two had L_{rp} equal to 1372 mm. For all specimens except for Specimens 36s-30 and 36s-30-P, L_{rp} was conservatively selected to minimize the strains on the beam at the end of the reinforcing plate. It will be shown that L_{rp} should be selected so that the strains at the end of the reinforcing plate remain under two-times the yield strain in order to avoid the limit state of beam local buckling.

The angle size and geometry was constant in all tests: L203x203x19 angles, 406 mm wide, and with $\sigma_{yn} = 345$ MPa. Two rows of two 32 mm A490 bolts connected the angle to the beam, and one row of four 32 mm A490 bolts connected the angle to the column at a distance of 137 mm from the bolt centerline to the bottom of the angle heel (resulting in $g_2 = 76$ mm, see Figure 2). Strain gages were installed in the column bolts to verify the pretension as well as to monitor the bolt force during testing.

Instrumentation was also installed to measure the local and global response of the specimens. Instruments were used to measure the applied loads, displacements, rotations, and strains in the beam. The imposed cyclic lateral displacement history was that recommended by SAC [19] for connection subassembly tests. Each load step had several cycles at a specified story drift (θ) as follows: 6 cycles at $\theta = 0.375\%$, 0.50% , and 0.75% , 4 cycles at $\theta = 1.0\%$, and 2 cycles at $\theta = 1.5\%$, 2% , 3% , and 4% . Most specimens were tested to 4% story drift as discussed later.

Table 2. Material Properties.**Material Properties**

A series of tests were conducted to establish the actual material properties. Uniaxial tension tests were conducted in accordance with ASTM standards [20]. Table 2 lists for the beam, column, angles, and reinforcing plates: (1) σ_y , the static yield stress as defined by Galambos [21], and (2) σ_u , the ultimate yield stress. Two-inch gage length, one-half inch diameter round tension coupons were used in all material tests. All of the steel for each specimen was ASTM A572 Grade 50, which has a specified minimum yield and ultimate stress of 345 MPa and 448 MPa, respectively.

	σ_y (MPa)	σ_u (MPa)
Beam Flange	362	498
Beam Web	414	527
Reinforcing Pl.	397	574
Column Flange	356	499
Column Web	345	496
Angles ^(a)	383	545
Angles ^(b)	358	523
PT Strands	1620 ^(c)	1900

The tension coupons for the beam flange, beam web, column flange, column web, and the reinforcing plates were taken from the longitudinal direction (i.e., parallel to the rolling direction).

The average of two similar tension test results is presented in Table 2 for these components. The tension coupons for the angles were taken in the transverse rolling direction (i.e., parallel to the direction of primary straining in the connection tests). The angles of Specimens 20s-18, 20s-18-W, 16s-45, 36s-30, and 36s-20-P were from the same heat. The angle material property values listed in Table 2 are the average of four tension test results, two from each angle leg.

- (a) All Specimens except 36s-30-P
 (b) Spec. 36s-30-P
 (c) Based on $0.85\sigma_u$

Each post-tensioning strand had an area of 140 mm² and consisted of a seven-wire strand protected with corrosion inhibitor grease and a 15-mm-diameter polypropylene sheath. Based on data from the manufacturer's material tests, conducted in accordance with ASTM A 416 [22], the modulus of elasticity and the tensile capacity were 199 GPa and 266 kN, respectively. The load-elongation curve indicates that yielding of the strands begins around 230 kN.

SUBASSEMBLY TEST RESULTS**General Behavior and Connection Moments**

The maximum story drift achieved for each specimen, θ_{max} , is given in Table 3 where θ_{max} is equal to the maximum column top displacement, Δ_{max} , divided by the column height of $h = 3962$ mm (i.e., $\theta_{max} = \Delta_{max}/h$). Most specimens were tested to 4% story drift. The limit states reached by each specimen are given in Table 3, and were as expected (see Table 1), with the exception of Specimen 36s-20-P. This specimen was expected to have angle fracture, however, it underwent two and one-half cycles of 4% story drift without connection failure as discussed later. The test of Specimen 36s-20-P was terminated after indications of web buckling in the beams, which were to be re-used for Specimen 36s-30-P. This onset of web buckling did not appear to affect the results of Specimen 36s-30-P. A photograph of Specimen 36s-20-P at 4% story drift is seen in Figure 5(a). It is seen that the angles are intact; when the applied lateral load was released the column returned to its plumb position as seen in Figure 5(b).

Table 3 also lists the experimentally observed decompression moment, $M_{d,exp}$, normalized by the nominal plastic moment capacity of the beam, $M_{p,n}$ (equal to 3282 kN-m). $M_{d,exp}$ was determined as the moment where the total strand force increased significantly, indicating strand elongation, as seen in Figure 6, which plots the total measured strand force, T , vs. $M/M_{p,n}$ for Specimen 20s-18. In Figure 6, M is the measured beam moment at the column face. Table 3 lists the average decompression moment from the east and west cycles. Specimens with smaller T_o had smaller $M_{d,exp}$ as expected from the relationship between T_o and $M_{d,exp}$ given by Equation 3. The experimental results are compared to Equation 3 later.

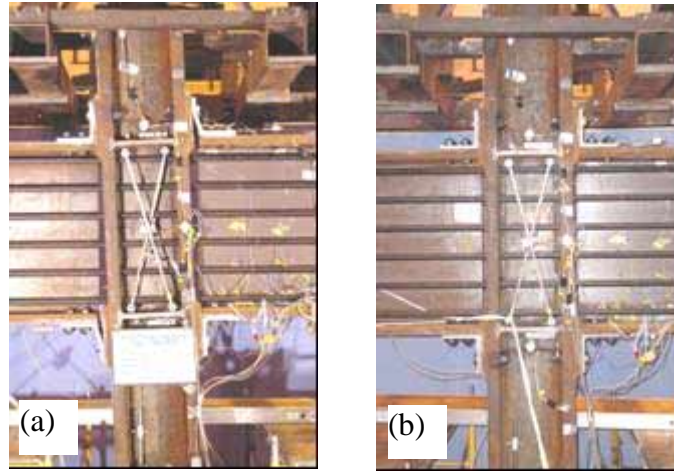


Figure 5. Specimen 36s-20-P (a) at $\theta = 4\%$ and (b) at end of test.

Table 3. Response of subassembly test specimens.

Specimen	T_o (kN)	θ_{max}	Limit State ^(a)	$\frac{M_{d,exp}}{M_{p,n}}$ ^(b)	$\frac{M_{max,exp}}{M_{p,n}}$ ^(b)	$\frac{T_{max,exp}}{T_u}$	$\theta_{r max}$ (rad)	$\Delta_{gap,max}$ (mm)
20s-18	1526	4.0%	AF	0.21	0.63	0.55	0.040	31
20s-18-W	1312	4.0%	AF	0.18	0.62	0.55	0.038	26
16s-45	3051	3.6%	SY	0.43	0.71	0.86	0.029	24
36s-30	4728	1.7%	BLB	0.68	0.82	0.52	0.006	6
36s-20-P	3194	4.0%	none	0.47	0.96	0.55	0.033	24
36s-30-P	4759	2.0%	BLB	0.65	0.93	0.58	0.013	12

(a) AF = Angle Fracture; SY = Strand Yield; BLB = Beam Local Buckling

(b) $M_{p,n} = 3282$ KN-m

Table 3 lists the maximum beam moment at the column face, $M_{max,exp}$, normalized by $M_{p,n}$. $M_{max,exp}$ is the maximum of the east beam and west beam moments. It is seen that Specimen 36s-20-P, which was tested to 4% story drift without reaching a limit state, reached 96% of $M_{p,n}$. Specimens 20s-18 and 20s-18-W, which were also tested to 4% story drift, reached only 63% and 62% of $M_{p,n}$, respectively. These specimens did not reach a value of $M_{max,exp}$ as large as Specimen 36s-20-P because they had a smaller T_o value and fewer strands. This caused the specimens to decompress earlier, and following decompression a smaller connection stiffness developed. Specimens 36s-30 and 36s-30-P attained relatively large values of $M_{max,exp}/M_{p,n}$, but the limit state of beam local buckling was reached at 2% story drift or less. This did not occur in Specimen 36s-20-P due to a smaller T_o . Specimen 16s-45 reached 71% of $M_{p,n}$ (at 3.6% story drift) when the test was terminated due to strand yielding and wire fracture.

Strand Behavior

The maximum PT force reached in the experiments, $T_{max,exp}$, normalized with respect to the strand capacity T_u , is listed in Table 3. Except for Specimen 16s-45, the strand forces remained under $0.60T_u$. The behavior of the strands is depicted in Figure 6 for Specimen 20s-18. The loss of prestress in each cycle is due to strand and anchorage seating. Figure 6 also demonstrates, as noted previously, that the strand force increases following decompression (due to strand elongation caused by connection gap opening).

Specimen 16s-45 had one or two wires fracture in a few strands before the test was ended at $\theta_{\max} = 3.6\%$. The estimated strand forces just before the wires fractured varied between 214 and 231 kN (i.e., $0.80T_u$ and $0.86T_u$, respectively), and were below the ultimate strand force of 266 kN (as reported by the strand manufacturer). These fractures occurred just outside the wedges, but within the anchor head. Examination of the fracture surfaces indicates that the fractures were ductile fractures caused by stress concentrations at the anchors and not caused by a notch or “bite” produced by the wedge.

Effects of T_o and N_s

Table 3 summarizes the maximum θ_r ($\theta_{r,\max}$) obtained for each specimen and the measured maximum gap opening ($\Delta_{\text{gap,max}}$). θ_r ranged from 0.029 to 0.040 radians and $\Delta_{\text{gap,max}}$ ranged from 24 to 31 mm for specimens reaching about 4% story drift. Deformations in the beams, columns, panel zone, and connection contribute to story drift. The connection component of story drift (i.e., θ_r) is largest for specimens with a smaller value of T_o (i.e., the smaller the T_o , the larger the θ_r). The effects of T_o are also illustrated by the $M - \theta_r$ plot shown in Figure 7, where M is the east beam moment at the column face. This figure shows the response of three specimens with different T_o values. It is seen that specimens with larger T_o values achieve a larger connection moment for a given θ_r . This is also observed in Table 3 by examining the trend of $M_{\text{max,exp}}$ and T_o . However, T_o , must not be too large in order avoid the beam local buckling limit state from occurring at relatively small story drift levels (as observed in Specimen 36s-30), and to also avoid strand yielding at a small story drift.

The axial stiffness of the strands (which is directly proportional to N_s) contributes the most to the stiffness of the connection after decompression. This can be seen by comparing the lateral load – displacement ($H - \Delta$) response for Specimens 16s-45 (which had 16 strands) and 36s-20-P (which had 36 strands) in Figure 8. These specimens had essentially the same T_o value (and therefore a similar $M_{d,\text{exp}}$) but different N_s values. Figure 8 shows that following decompression, the stiffness of Specimen 36s-20-P is significantly greater than that of Specimen 16s-45, which had 20 fewer strands. Specimen 16s-45 was not tested to as large a story drift as Specimen 36s-20-P since, as noted above, some wires in the strands fractured. This comparison demonstrates two advantages to using a larger number of strands to achieve a selected level of

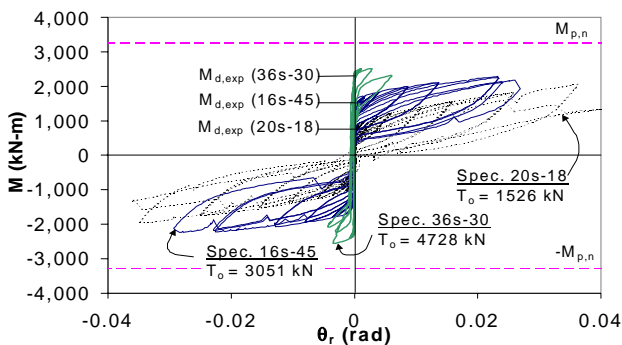


Figure 7. Moment – relative rotation response of Specimens 20s-18, 16s-45, and 36s-30.

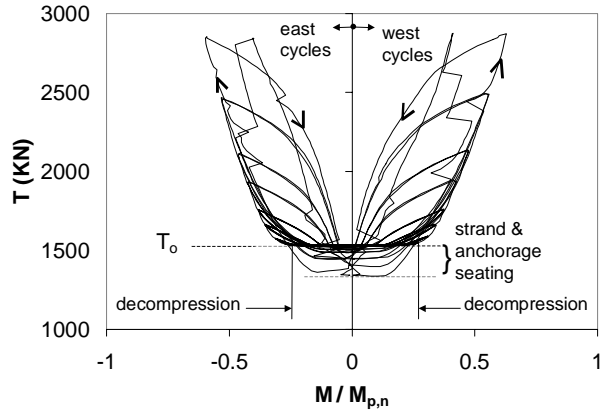


Figure 6. Cyclic behavior of PT strand force, Specimen 20s-18.

T_o ; (1) greater strength is achieved because of a larger stiffness after decompression, and (2) greater deformation capacity (i.e., θ_r) is available since the strands have a smaller initial force, and therefore a larger margin for increasing the strand force without fracture or yield of the strands.

Figure 8 also indicates that Specimens 36s-20-P and 16s-45 have the same initial lateral stiffness (prior to decompression), which is comparable to that of a welded connection specimen, K_{welded} , as established by Ricles et al. [23]. In general, prior to decompression, all of the PT connection

specimens had an initial stiffness similar to that of a welded connection.

Beam Local Buckling and Beam Strains

Table 3 shows that Specimens 36s-30 and 36s-30-P were tested to a maximum story drift of 1.7% and 2%, respectively. However, the peak maximum load, H_{max} , was attained at 1.3% and 1.9% story drift for Specimens 36s-30 and 36s-30-P, respectively. The deterioration in load carrying capacity on these specimens is attributed to beam flange and web local buckling. A longer reinforcing plate delays the onset of local beam flange and web local buckling, and Specimen 36s-30-P with a reinforcing plate 458 mm longer than that of Specimen 36s-30, achieved an additional 0.6% story drift before local buckling developed. These specimens had a large T_o value and therefore a large $M_{d,exp}$. The combined stresses on the beam due to moment and axial load (due to the post-tensioning) caused the beam to buckle locally before a large θ_r was reached. The self-centering capability of the PT connection is lost after the onset of beam local buckling, where Specimens 36s-30 and 36s-30-P both had a residual column top deflection of about 18 mm when the lateral load was removed.

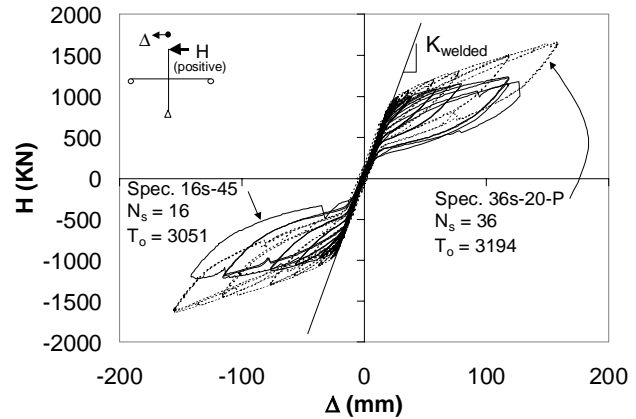


Figure 8. Lateral load – displacement response of Specimens 36s-20-P and 16s-45.

Garlock [16] shows that for a distance from the column face greater than the reinforcing plate length, L_{rp} , the strains vary nearly linearly through the beam depth, suggesting that plane sections remain plane. However, within the length of the reinforcing plate, plane sections do not typically remain plane. Exactly at the end of the reinforcing plate, the strains vary linearly across the beam depth except at the outermost compressive fiber. At this point, the strains are relatively large indicating that strain concentrations form in the beam flange at the end of the reinforcing plate.

Local flange and web buckling results in flange and web distortion, which leads to shortening of the beam, which in turn leads to a loss of post-tensioning force. Loss of post-tensioning results in a loss of connection strength, and if the angles also fracture, the gravity load capability of a PT frame could be compromised. Therefore, for the development of design criteria, it is important to identify the strains producing the flange and web distortion leading to local buckling and a loss in post-tension force. In these experiments, it was generally found that if a lateral drift was imposed that resulted in the strain exceeding two-times the yield strain, ϵ_y , near the end of the reinforcing plates, then the beam flanges developed a significant rate of increase in plastic strain indicating the onset of beam local buckling. This strain value of $2\epsilon_y$ is less than expected based on experiments by Ricles et al. [23], which included only bending in the beam. The relatively low value in the current specimens is attributed to the stress concentrations at the end of the reinforcing plate and the combination of axial force and bending in the beam.

Angle Behavior

Specimens 20s-18 and 20s-18-W reached the limit state of angle fracture. All four angles fractured in the fillet of the leg attached to the column at the end of two cycles of 4% story drift (θ). The response of Specimen 20s-18-W (with welded angles) was the same as Specimen 20s-18, suggesting that the impact forces caused by slip of the angles relative to the beam did not affect the angle's fatigue life.

The total initial strand force, T_o , strongly influences the limit state of angle fracture. A smaller T_o , leads to earlier decompression, and therefore leads to more plastic deformation of the angles leading to angle fracture. An example of the influence of T_o can be seen by comparing the performance of Specimens 20s-18 ($T_o = 1526$ kN) and Specimen 36s-20-P ($T_o = 3194$ kN). Both specimens were expected to reach the limit state of angle fracture (see Table 1) based on previous research [4]. Yet Specimen 20s-18, with about half the T_o value of Specimen 36s-20-P, had all four angles fracture at the end of two cycles of 4% story drift, whereas Specimen 36s-20-P did not fracture any angles after two and one-half cycles of 4% story drift. This is attributed to the fact that the angles of Specimen 20s-18 underwent more accumulated plastic strain due to earlier decompression.

COMPARISION WITH EXPECTED RESPONSE

$M_{d,exp}$ is compared to the predicted decompression moment, $M_{d,th}$, in Table 4. $M_{d,th}$ is computed using Equation 3 where the resultant of the contact force is assumed to act at the center of the reinforcing plate thickness. $M_{d,exp}$ is determined as the moment where the slope of the total strand force versus moment curve increased significantly, as shown in Figure 6. Table 4 shows that the correlation between $M_{d,exp}$ and $M_{d,th}$ is good, where the values of $M_{d,exp}/M_{d,th}$ are within 5% of unity.

Figure 9 compares the predicted total strand force, T_{th} , based on Equation 5 with the envelope of the measured strand force vs. story drift ($T_{exp} - \theta$) for Specimen 20s-18 from the experiment. The results from Equation 5 use the measured θ_r and are calculated in two ways: (1) The first includes the effects of strand and anchorage seating by using the strand force at the beginning of every load cycle (using measured values) as T_o ; and (2) neglecting the effects of anchorage seating by using a constant value for T_o equal to the strand force measured at the beginning of the test. It is seen that when strand and anchorage seating is accounted for, the correlation to the experimental results is better than when it is neglected. However, strand and anchorage seating does not significantly affect the results. Table 4 compares T_{th} , to T_{exp} , at 3% story drift for all specimens that reached or exceeded 3% story drift. T_{th} is based on Equation 5 with θ_r equal to the measured θ_r at 3% story drift, and includes the effects of strand and anchorage seating. Again, good correlation is seen between the experimental and analytical results, where T_{exp}/T_{th} values are within 5% of unity.

Table 4 also compares the predicted connection moment, M_{th} , to the experimentally measured connection moment, M_{exp} , at 3% story drift for all specimens that reached or exceeded 3% story drift. M_{th} , is estimated from Equation 2 as follows:

- θ_r is equal to the measured θ_r for the east beam at 3% story drift;
- F_{fd} is equal to zero (for a subassembly) and therefore P is equal to T , calculated using Equation 5 as described above using the measured value of T_o ;
- M_a^T and M_a^C (in Equation 2) are equal to $\beta M_{a,p}$ and $M_{a,p}$, respectively, where β is given in Equation 4;
- V_a is from Equation 4, with Δ_{gap} equal to $d_3\theta_r$;
- d_1 and d_2 are as defined in Figure 3 assuming the resultant of the contact force acts at the center of the reinforcing plate thickness.

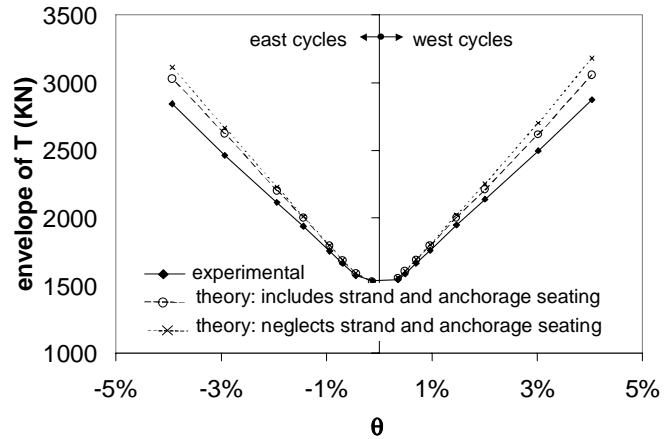


Figure 9. Experimental vs. theoretical strand force (Specimen 20s-18).

Table 4. Comparison of response.

Specimen	$\frac{M_{d,exp}}{M_{d,th}}$	$\frac{T_{exp}}{T_{th}^{(a)}}$	$\frac{M_{exp}}{M_{th}^{(a)}}$	
			east beam	west beam
20s-18	0.98	0.94	0.88	0.92
20s-18-W	0.97	0.96	0.94	0.96
16s-45	0.99	0.95	0.90	0.94
36s-30	1.01	-	-	-
36s-20-P	1.03	0.94	0.88	0.93
36s-30-P	0.95	-	-	-

(a) includes the effects of strand and anchorage seating

(b) T_{exp}/T_{th} and M_{exp}/M_{th} are evaluated at $\theta = 3\%$

It is seen that M_{th} tends to overestimate M_{exp} , but the difference is less than 12%. Some of this discrepancy is from the overestimation of T (see Table 4), and the rest is from an overestimation of the angle force V_a . V_a could not be directly measured in the tests and is therefore not compared to Equation 4.

SUMMARY AND CONCLUSIONS

The results of six full-scale tests show that PT steel connections specimens subjected to severe cyclic loading exhibit stable self-centering hysteretic behavior when beam local buckling and strand yielding do not occur. The beams and column remain essentially elastic, with inelastic deformations concentrated in the connection angles. Beam local buckling prevents the specimen from self-centering and limits the ductility. Therefore the connection should be designed to avoid this limit state. This limit state can be delayed by using longer reinforcing plates and/or by using a smaller initial post-tensioning force. To prevent strand yielding, a larger number of strands, with a smaller initial post-tensioning force per strand, is recommended.

A larger connection moment and greater ductility were achieved in the connections with a larger number of strands. The greater the number of strands, the larger the connection stiffness after decompression and angle yielding, which results in a larger connection moment. Also, the greater the number of strands, the less likely the strands will yield since the initial post-tensioning force per strand is likely to be smaller.

For specimens with a smaller total initial post-tensioning force, T_o , the connection rotation, θ_r , had a larger contribution to the story drift than the specimens with a larger T_o . For a smaller T_o , smaller elastic deformations occur in the beam and column. Specimens with a smaller T_o decompress earlier and have a larger relative rotation in the connection, θ_r , at a specified story drift level, leading to a greater potential for angle fracture.

Plane sections do not remain plane through the beam depth within the length of the reinforcing plate, but do remain plane beyond the end of the reinforcing plate. It was generally found that when the strain exceeded two-times the yield strain, ϵ_y , in the beam flanges near the end of the reinforcing plate, the beam flanges developed a significant increase of plastic strain indicating the onset of beam local buckling.

Predictive equations were presented to estimate the decompression moment, maximum connection moment, and maximum strand force. The equations were found to produce results that were in good agreement with the experimental results.

Garlock [16] performed nonlinear time-history analyses of six-story four-bay steel MRFs with PT connections under earthquake loading. Comparing the seismic demands obtained from these analyses, with the test results reported herein, it is concluded that PT steel connections can provide adequate strength, stiffness, and drift capacity for a MRF subject to earthquake loading.

ACKNOWLEDGEMENTS

The research reported herein was supported by the National Science Foundation (Dr. Ken Chong and Dr. Ashland Brown cognizant program officials) and a Lehigh University Fellowship. The research was also supported by a grant from the Pennsylvania Department of Community and Economic Development through the Pennsylvania Infrastructure Technology Alliance (PITA) program. The opinions expressed in this paper are those of the authors and do not necessarily reflect the views of the sponsors.

REFERENCES

1. Roeder, C.W. "State of the Art Report Connection Performance," Federal Emergency Management Agency (FEMA) *Bulletin No. 355D*, Washington, D.C., 2000.
2. Garlock, M, Ricles, J., and Sause, R. "Experimental Studies on Full-Scale Post-Tensioned Steel Connections" (submitted to *Journal of Structural Engineering* in Nov. 2003).
3. Garlock, M, Ricles, J., and Sause, R. "*Design and Behavior of Post-Tensioned Steel Moment Frames*" 13th World Conference on Earthquake Engineering (13WCEE), Vancouver, BC Canada August 2004.
4. Garlock, M, Ricles, J., and Sause, R. "Cyclic Load Tests and Analysis of Bolted Top-and-Seat Angle Connections," *Journal of Structural Engineering*, ASCE 129(12), 2003: 1615-1625.
5. Cheok, G. and Lew, H.S. "Model Precast Concrete Beam-to-Column Joints Subject to Cyclic Loading," *PCI Journal*, Precast/Prestressed Concrete Institute, v. 38, No. 4, July-August 1993: 80-92.
6. Cheok, G. and Stone, W. "Performance of 1/3-Scale Model Precast Concrete Beam-Column Connections Subjected to Cyclic Inelastic Loads – Report No. 4," *NISTIR 5436*, National Institute of Standards and Technology, NIST, Gaithersburg, MD, June 1994.
7. El-Sheikh, M.T., Sause, R., Pessiki, S., and Lu, L.-W. "Seismic Behavior and Design of Unbonded Post-Tensioned Precast Concrete Frames," *PCI Journal*, 44 (3), May/June 1999: 54-71.
8. Rojas, P., Garlock, M., Ricles, J., Sause, R. "Reducing Seismic Damage In Steel Frames Using Post-Tensioning," in *Proceedings of the 7th U.S. National Conference on Earthquake Engineering (NCEE)*, Boston, MA. 2002.
9. Rojas, P. "Seismic Analysis and Design of Post-Tensioned Friction Damped Connections for Steel Frames", Ph.D. Dissertation, Department of Civil and Environmental Engineering, Lehigh University, Bethlehem, Pa., May 2003.
10. Christopoulos, C., Filiatrault, A., Uang, C.-M., Folz, B." Posttensioned Energy Dissipating Connections for Moment-Resisting Steel Frames", *Journal of Structural Engineering*, ASCE, 128(9) 2002: 1111-1120.
11. Christopoulos, C., Filiatrault, A., and Uang, C.-M. "Behavior of Steel Moment Resisting Frames with Post-Tensioned Energy Dissipating Connections," in *Proceedings of the 7th U.S. National Conference on Earthquake Engineering (NCEE)*, Boston, MA 2002.

12. Christopoulos, C., Filiatrault, A., and Uang, C.-M. "Seismic Demands on Post-Tensioned Energy Dissipating Moment-Resisting Steel Frames," in *Proceedings of Steel Structures in Seismic Areas (STESSA)*, Naples, Italy 2003.
13. Christopoulos, C., Filiatrault, A., Folz, B. "Seismic Response of Self-Centering Hysteretic SDOF Systems," *Earthquake Engineering and Structural Dynamics*, John Wiley & Sons, Ltd., Vol. 31, 2002: 1131-1150.
14. Ricles, J., Sause, R., Peng, S.W., and Lu, L.W. "Experimental Evaluation of Earthquake Resistant Posttensioned Steel Connections," *Journal of Structural Engineering*, ASCE, 128(7), 2002: 850-859.
15. Ricles, J., Sause, R., Garlock, M, and Zhao, C. "Post-Tensioned Seismic Resistant Connections for Steel Frames," *Journal of Structural Engineering*, ASCE, 127(2), 2001: 113-121.
16. Garlock, M. "Full-Scale Testing, Seismic Analysis, and Design of Post-Tensioned Seismic Resistant Connections for Steel Frames," *Ph.D. Dissertation*, Civil and Environmental Engineering Dept., Lehigh University, Bethlehem, PA., 2002.
17. *Seismic Provisions for Structural Steel Building*. AISC, Chicago, Illinois, 1997.
18. *Load and Resistance Factor Design Specification for Structural Steel Buildings, 3rd Ed.* AISC, Chicago, Illinois, 2000.
19. SAC Joint Venture. "Protocol For Fabrication, Inspection, Testing, and Documentation of Beam-Column Connection Tests and Other Experimental Specimens", *Report No. SAC/BD-97/02*, Version 1.1, October 1997.
20. American Society for Testing and Materials. "Standard Methods for Tension Testing of Metallic Materials." *ASTM Designation E8-91*, Philadelphia, 1991.
21. Galambos, T.V. *Guide to Stability Design Criteria for Metal Structures*, 5th Edition, John Wile & Sons, Inc., 1998.
22. American Society for Testing and Materials. "Standard Specification for Steel Strand, Uncoated Seven-Wired for Prestressed Concrete," *ASTM Designation No. A416-94*, Philadelphia, 1997.
23. Ricles, J.M., Mao, C., Lu, L.-W., Fisher, J.W. "Inelastic Cyclic Testing of Welded Unreinforced Moment Connections," *Journal of Structural Engineering*, ASCE, 128(4), 2002: 429-440.